Redox Biology 13 (2017) 568–580

Contents lists available at ScienceDirect

Redox Biology

journal homepage: www.elsevier.com/locate/redox

Research Paper

Identification of transcriptome signature for myocardial reductive stress

Justin M. Quiles[a,1], Madhusudhanan Narasimhan[b,1], Timothy Mosbruger[c], Gobinath Shanmugam[a], David Crossman[d], Namakkal S. Rajasekaran[a,c,e,*,1]

[a] Cardiac Aging & Redox Signaling Laboratory, Division of Molecular & Cellular Pathology, Department of Pathology, The University of Alabama at Birmingham, Birmingham, AL 35294, USA
[b] Department of Pharmacology and Neuroscience, Texas Tech University Health Sciences Center, Lubbock, TX 79430, USA
[c] Division of Cardiovascular Medicine, Department of Medicine, University of Utah School of Medicine, Salt Lake City, UT 84132, USA
[d] Heflin Center for Genomic Sciences, The University of Alabama at Birmingham, Birmingham, AL 35294, USA
[e] Center for Free Radical Biology, The University of Alabama at Birmingham, Birmingham, AL 35294, USA

ABSTRACT

The nuclear factor erythroid 2 like 2 (Nfe2l2/Nrf2) is a master regulator of antioxidant gene transcription. We recently identified that constitutive activation of Nrf2 (CaNrf2) caused reductive stress (RS) in the myocardium. Here we investigate how chronic Nrf2 activation alters myocardial mRNA transcriptome in the hearts of CaNrf2 transgenic (TG-low and TG-high) mice using an unbiased integrated systems approach and next generation RNA sequencing followed by qRT-PCR methods. A total of 246 and 1031 differentially expressed genes (DEGs) were identified in the heart of TGL and TGH in relation to NTG littermates at ~ 6 months of age. Notably, the expression and validation of the transcripts were gene-dosage dependent and statistically significant. Ingenuity Pathway Analysis identified enriched biological processes and canonical pathways associated with myocardial RS in the CaNrf2-TG mice. In addition, an overrepresentation of xenobiotic metabolic signaling, glutathione-mediated detoxification, unfolded protein response, and protein ubiquitination was observed. Other, non-canonical signaling pathways identified include: eNOS, integrin-linked kinase, glucocorticoid receptor, PI3/AKT, actin cytoskeleton, cardiac hypertrophy, and the endoplasmic reticulum stress response. In conclusion, this mRNA profiling identified a "biosignature" for pro-reductive (TGL) and reductive stress (TGH) that can predict the onset, rate of progression, and clinical outcome of Nrf2-dependent myocardial complications. We anticipate that this global sequencing analysis will illuminate the undesirable effect of chronic Nrf2 signaling leading to RS-mediated pathogenesis besides providing important guidance for the application of Nrf2 activation-based cytoprotective strategies.

1. Introduction

The cap 'n' collar (CNC) basic leucine zipper transcription factor nuclear factor erythroid 2 like 2 (Nfe2l2/Nrf2) is a master regulator of antioxidant (ARE) and electrophile (EpRE) response elements that affords cytoprotection from xenobiotics and free radical accumulation [1]. Under basal conditions, Nrf2 is bound by its repressor, kelch-like-ECH associated protein 1 (Keap1) through interaction at its Neh2 domain and is anchored to the actin cytoskeleton where it undergoes ubiquitination and proteasomal degradation [2–4]. However, upon oxidative stress or electrophilic stimulation, Keap1 binding is disrupted, facilitating Nrf2 stabilization and subsequent nuclear translocation. Upon nuclear entry, Nrf2 heterodimerizes with transcriptional cofactors to bind cis-regulatory elements at the promoters of various cytoprotective genes and modulates gene transcription.

An increasingly diverse list of mechanisms responsible for prompting Keap1 dissociation and Nrf2 nuclear import has emerged in recent years. Chemical and pharmacological inducers of phase II enzyme activity react with crucial cysteine thiols on Keap1, thereby preventing Nrf2 binding [5]. Non-canonical autophagy signaling has been shown to exhibit cross-talk with Nrf2 as phosphorylated p62 competitively interferes with Keap1-Nrf2 interaction [6]. Furthermore, endogenous protein kinase activity such as PI3K and MAPK/ERK act upstream of Nrf2 target gene expression [7,8]. Interestingly, PERK activation as a result of endoplasmic reticulum (ER) stress and protein aggregation can phosphorylate Nrf2, thereby facilitating its role as an

* Correspondence to: Cardiac Aging & Redox Signaling Laboratory, Center for Free Radical Biology, Division of Molecular & Cellular Pathology, Department of Pathology, UAB|The University of Alabama at Birmingham, BMR2 Room 533|901 19th Street South, Birmingham, AL 35294-2180, USA.
E-mail address: rajnsr@uabmc.edu (N.S. Rajasekaran).
[1] These authors contributed equally.

http://dx.doi.org/10.1016/j.redox.2017.07.013
Received 8 July 2017; Received in revised form 20 July 2017; Accepted 20 July 2017
Available online 24 July 2017

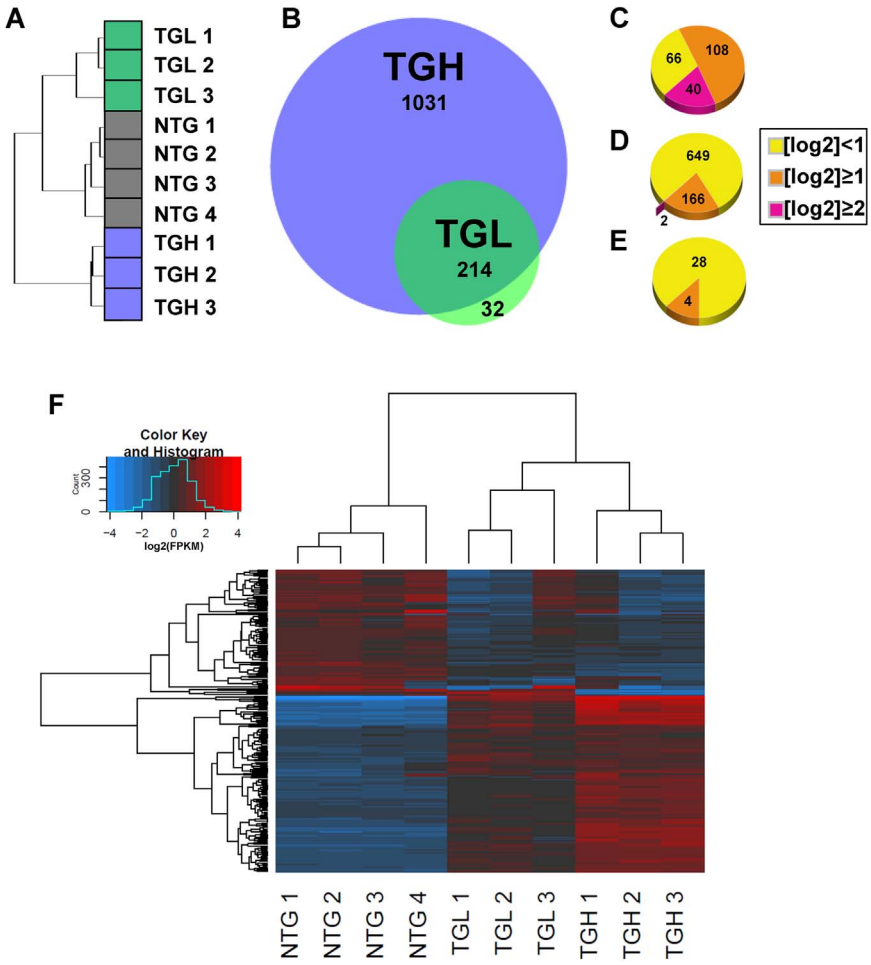

Fig. 1. Dose-dependent effects of CaNrf2 transgene expression. A) Hierarchal clustering analysis for all samples used in next-generation RNA sequencing (RNAseq) (n = 3–4/group). Clustering was performed for all genes with FPKM ≥ 1 in at least two samples B) area proportional Venn diagram depicting the number of differentially expressed genes (DEG's) identified by RNAseq of CaNrf2 transgenic-low (TGL) and transgenic-high (TGH) hearts. C, D, E) DEG's shared between groups (C), unique to TGH (D), and TGL (E) partitioned according to log2 fold-change (FC). F) Hierarchal clustering heat map of $\log_2$ transformed FPKM values for all 214 DEGs shared by TGL and TGH groups. Each column represents individual biological replicates in respective groups of transgenic mice and each row represents a DEG wherein red denotes upregulation and blue downregulation according to the color scale shown (top). Expression values are mean-centered. (For interpretation of the references to color in this figure legend, the reader is referred to the web version of this article.)

unfolded protein response (UPR) factor [9,10]. Thus, Nrf2 signaling has widespread functions with implications in autophagy, apoptosis, and the UPR. Although decades of antioxidant signaling research have extensively delineated roles for Nrf2 in redox homeostasis, recent reports from our laboratory have uncovered intriguing effects of Nrf2 mediated induction of phase II detoxifying enzymes involved in glutathione biosynthesis and oxidoreductase activities on protein quality control and reductive stress [11–13]. Along these lines, we have demonstrated a paradoxical role for Nrf2 in potentiating cardiotoxic effects through aberrant activation of antioxidant responses causing reductive stress in mice overexpressing cardiac-specific human R120G αB-crystallin [11,12]. Although protein aggregates are a common site for oxidative events, the hR120GCryAB mutant mice with severe protein aggregation cardiomyopathy displayed substantial Keap1 sequestration in mutant protein aggregates resulting in sustained Nrf2 nuclear import with a robust redox shift towards the reductive side [12]. Thus, a certain oxidative threshold and/or biochemical reactions involving reactive oxygen species (ROS) are integral for carrying out a wide range of cellular functions critical to maintaining vascular tone and cardiac function, including but not limited to; energy metabolism, cell proliferation, calcium handling, immune modulation, as well as several intracellular signal transduction pathways [14,15]. Thus, maintaining redox balance is a crucial prerequisite to reinforce the normal physiological and biological aspects in the cardiovascular system. Although Nrf2 is still regarded widely as a promising drug target, we believe more research is needed to validate its activation as a viable strategy using sustained and/or chronic Nrf2 activation models. In particular, little is known about its sustained activation on the cardiac system.

To determine this, we have utilized transgenic mice with cardiac-specific constitutive Nrf2 signaling (CaNrf2). This is a genetic model of antioxidant abundancy wherein, under the control of a myosin heavy chain promoter, the transgenic construct lacks a functional Neh2 domain that prohibits Keap1 repression resulting in constitutive Nrf2 activation [16]. Mouse lines exhibiting moderate (TGL) and high (TGH) levels of transgene expression were maintained and cardiac RNA was subjected to high-throughput RNA sequencing. A comparison of TGL and TGH groups demonstrated a dose-dependent effect of Nrf2 activity on the number and magnitude of differentially expressed genes (DEGs), with 817 unique DEGs belonging only to TGH. Real-time qPCR validation and Ingenuity Pathways Analysis (IPA) elucidated a unique reductive stress transcriptional signature consistent with pronounced increases in glutathione synthesis, impaired protein quality control, and cardiovascular pathology. We believe that the CaNrf2 model provides a global perspective of genetic and biochemical relationships to help define how alterations in gene expression may underlie myocardial perturbations in the previously unknown condition of cardiac reductive stress. More generally, this unique mouse line and the transcriptomic data will allow investigators in the future to explore novel expression patterns relevant to cardiac diseases characterized by redox dysregulation, particularly ‘Reductive Stress’.

2. Results

2.1. Rationale for using constitutively active Nrf2 (CaNrf2) to identify the transcriptome signature for reductive stress in mouse myocardium

Clinical trials with antioxidant agents and/or manipulating the expression of Nrf2 that protect against oxidative stress in human disorders

have often resulted in inconsistent results [17,18]. The mechanisms associated with these inconsistent effects in cardiovascular complications are largely unknown, in part due to lack of explicit and suitable *in vivo* models. In this context, we used a previously generated heart-specific genetic mouse models with pro-reductive and reductive stress conditions through expressing varying levels of constitutively active Nrf2 (CaNrf2), a master transcriptional regulator of antioxidant genes [16]. This is essentially a genetically engineered novel mouse model with abundant endogenous levels of antioxidant(s) that would mimic the chronic antioxidant supplementation model and its effects. Mouse α-myosin heavy chain (αMHC) promoter directed the expression of CaNrf2 in the heart and yielding two different transgenic lines that express either low (TGL) or high (TGH) levels of CaNrf2. Details of generating CaNrf2 transgenic mouse models were described in our recent publication [16].

2.2. Dose-dependent effects of CaNrf2 transgene expression

Cardiac transcriptional signatures clustered in a genotype-specific manner following RNA sequencing (RNAseq) (Fig. 1A). However, analysis of sequencing data revealed pronounced genetic dysregulation in CaNrf2 mouse hearts according to the level of transgene expression. While moderate CaNrf2 expression in TGL mice generated 246 differentially expressed genes (DEGs), higher transgene expression in TGH mice allowed for the detection of a striking 1031 DEGs (Fig. 1B). Importantly, CaNrf2 TGL expression profiles were congruent with TGH mice as 87% of DEGs overlapped with the TGH transcriptome (Fig. 1B). A vast majority of the most robustly altered DEGs were shared between TGL and TGH groups as 40 of the 42 genes exhibiting a $\log_2$ expression ratio of at least 2.0 were consistent among both groups (Fig. 1C). Although the TGL expression profile conformed to TGH, the increased transgene expression in TGH group resulted in 817 unique DEGs. Further, many of these genes were markedly dysregulated in TGH mice as 166 DEGs exhibited a $\log_2$ expression ratio greater than 1.0 following RNAseq analysis (Fig. 1D). Conversely, only 4 unique DEGs in the TGL group demonstrated such fold changes (Fig. 1E). A closer examination of the FPKM values for shared DEGs amongst TGL and TGH samples further revealed the dose-dependent nature of genetic disarray in the CaNrf2 model (Fig. 1F).

2.3. Canonical pathways and biological functions associated with Nrf2 mediated cardiac reductive stress

DEGs were filtered through the Ingenuity Pathway Analysis (IPA) to uncover enriched canonical pathways (Fig. 2A) and biological functions (Fig. 2B) in the CaNrf2 reductive stress (RS) model. Unsurprisingly, the Nrf2-mediated redox response was the most significantly activated canonical pathway in the TGH myocardium (Fig. 2A). In TGL mice, this canonical pathway shared the top ranking with the closely related xenobiotic metabolism pathway (Fig. 2A). In addition to oxidative stress and xenobiotic metabolism, hearts of CaNrf2 mice displayed pronounced increases in 9 canonical mechanisms related to antioxidant and glutathione cellular detoxification (Fig. 2A). Taken together, the prevalence of these signaling cascades are suggestive of Nrf2 mediated enhancements of reducing power in transgenic hearts.

Both TGL and TGH groups presented cardiac hypertrophy and atherosclerosis signaling, however, the phenotype of TGH mice appeared more severe as 4 additional cardiac pathology pathways emerged in this group (Fig. 2A). The robust integrin-linked kinase (ILK) activity in TGH mice may explain a more pronounced cardiac phenotype as this cascade has been reported to positively regulate hypertrophy [19]. Alternatively, dysregulated calcium dynamics and NFAT signal transduction may underlie the hypertrophic phenotype evident in TGH mice (Fig. 2A). Since impaired calcium dynamics can stimulate cell death mechanisms [20], it is not surprising that CaNrf2 mice may exhibit activated apoptosis and death receptor pathways (Fig. 2A). In support of previous findings of protein kinase modulation of Nrf2 activity [7,8], CaNrf2 mice displayed significant changes in the PI3K/AKT, ERK/MAPK and AMPK signaling pathways (Fig. 2A).

IPA analysis of the CaNrf2 model demonstrated perturbations in 9 major biological functions coinciding with over-represented pathways (Fig. 2B). Specified annotations within each biological function allowed for the identification of potential disease phenotypes associated with TGL and TGH transcriptomes (Fig. 2B). Free radical scavenging and drug metabolism functions were similarly enhanced in TGL and TGH mice with corresponding annotations linked to reactive oxygen species removal and glutathione metabolism (Fig. 2B). Genes involved in cellular compromise and post-translational modification functions, as well as protein ubiquitination and the ER stress signaling pathway, were dose-dependently dysregulated in the TGH group (Fig. 2A and B). In particular, the DEG profile was strongly associated with stress response, protein conformational modification, and protein folding disease annotations only in TGH mice (Fig. 2B). Interestingly, an altered cellular assembly and organization processes in CaNrf2 hearts with disease annotations related to cytoplasm development, cytoskeletal assembly and actin filament formation was noted (Fig. 2B). This function matches the heightened actin cytoskeletal signaling observed (Fig. 2A) and has broad implications for cardiac function [21]. Despite a more striking response in TGH, the transcriptional signatures of both groups revealed complications in muscular development, cardiovascular system function, and a cardiovascular disease characterized by underlying hypertrophic morphological changes, altered contractility, and cell death (Fig. 2B).

2.4. Augmented oxidoreductase activity and glutathione metabolism

The top 25 DEGs within each of the nine major biological functions altered in the cardiac reductive stress model were compared by their relative expression to non-transgenic (NTG) control mice, and 4 genes were chosen for real-time qPCR validation from each category. Significant correlations were observed between RNAseq derived $\log_2$ expression ratios and $\log_2$ transformed mean fold-change observed in validation experiments (Supplementary material Fig. 2D).

Constitutive Nrf2 activity increased the expression of a variety of redox enzymes involved in free radical scavenging including catalase (*Cat*), glutathione peroxidase 3 (*Gpx3*), monoamine oxidase A (*Maoa*), thioredoxin reductase 1 (*Txnrd1*), thioredoxin 1 (*Txn1*), peroxiredoxin 6 (*Prdx6*) and phosphogluconate dehydrogenase (*Pgd*) (Fig. 3A and data not shown). Importantly, a regulator of G-protein signaling 6 (*Rgs6*), which is required for ROS induced cardiomyopathy following doxorubicin administration [22,23], was robustly downregulated in TGH mice further illustrating a prevailing reducing environment in CaNrf2 hearts (Fig. 3A). In addition, the expression of genes involved in iron homeostasis such as Hephaestin (*Heph*) and the transferrin receptor (*Tfrc*) was upregulated in reductive stress hearts indicating a potential for continuous iron uptake leading to toxicity (Fig. 3A). *Heph*, *Prdx6*, *Tfrc*, and the serine (or cysteine) peptidase inhibitor *Serpina3c* were selected for qPCR validation. Dose-dependent increases were evident in *Heph, Prdx6* and *Serpina3c* Expression (Fig. 3B). While mean *Heph* mRNA was 6-fold higher in TGL than controls, TGH mice exhibited nearly a 19-fold increase (Fig. 3B). Similarly, *Serpina3c* expression was 10 and 33-fold higher in TGL and TGH groups, respectively (Fig. 3B). *Prdx6* mRNA was 4-fold greater in the TGH group relative to NTG controls (Fig. 3B).

IPA's biological function of drug metabolism included many genes involved in cellular detoxification. Substantial increases in the expression of the glutamate-cysteine ligase modifier subunit (*Gclm*), gamma-glutamyltransferase 5 (*Ggt5*), glutathione reductase (*Gsr*), glutathione synthetase (*Gss*), glutathione S-transferases, alpha 3 and 4 (*Gsta3*, *Gsta4*), and glutathione S-transferases, mu 1 and 4 (*Gstm1*, *Gstm4*) were detected in TGH mice (Fig. 3C). However, in TGL mice, only *Gclm*, *Gsta3*, and *Gstm1* were elevated implying a certain threshold of Nrf2

Fig. 2. Canonical pathways and biological functions associated with Nrf2 mediated cardiac reductive stress. A) Heat map illustrating Log transformed p-values of significantly enriched canonical pathways obtained from Ingenuity Pathway Analysis (IPA). B) Log transformed p-values of disease annotations encompassing 9 major biological functions altered in reductive stress mice.

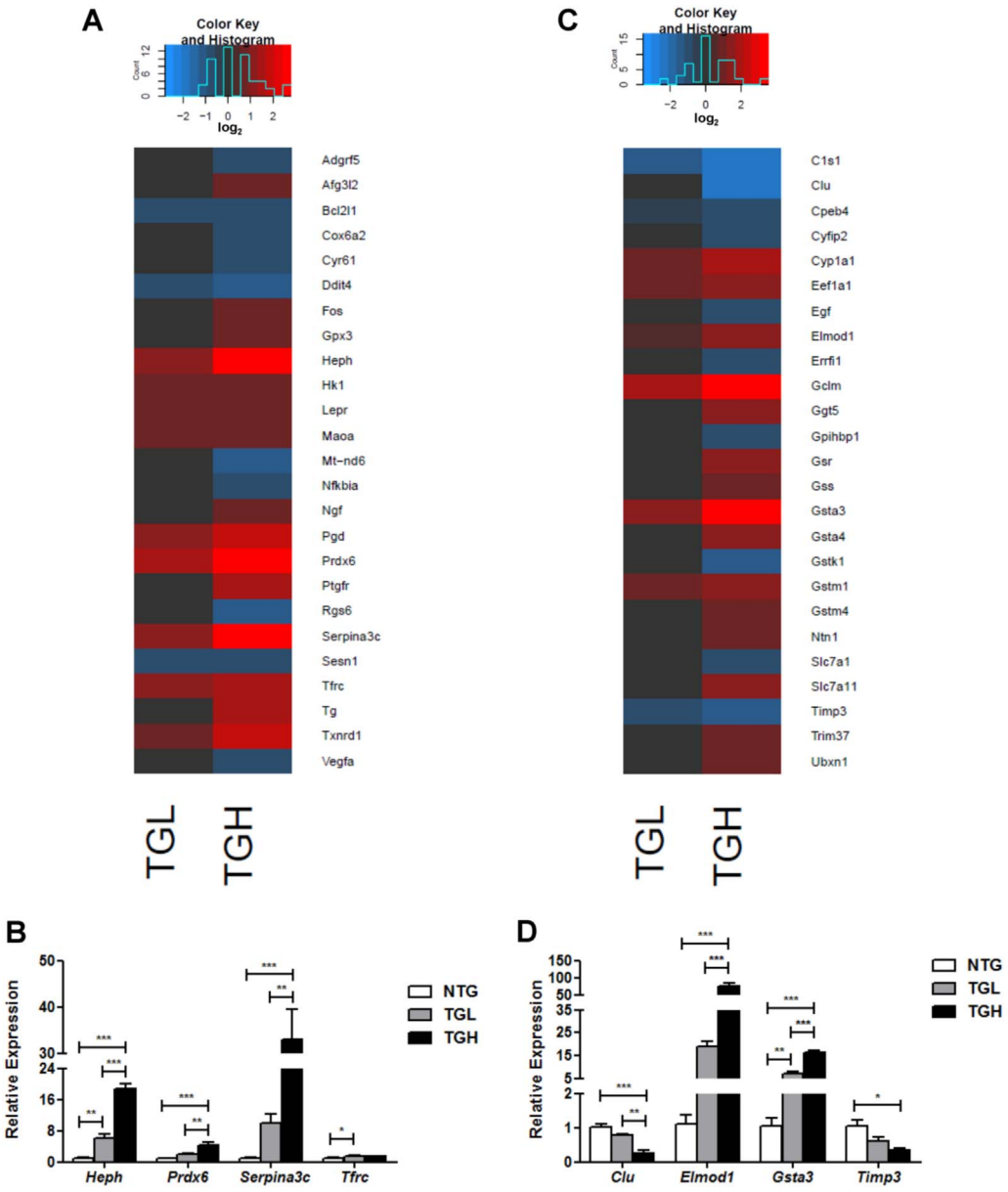

Fig. 3. Augmented oxidoreductase activity and glutathione metabolism. A) Heat map illustrating RNAseq derived log2 expression changes of the top 25 DEG's contained within IPA's biological function of free radical scavenging. Red values indicate upregulation, black values indicate either unchanged or insignificant change, and blue indicates downregulated expression when compared to non-transgenic mice (NTG). B) Real-time qPCR validation of 4 genes within the free radical scavenging category. C) Heat map illustrating RNAseq derived log2 expression changes of the top 25 DEG's contained within IPA's biological function of drug metabolism and protein synthesis. Real-time qPCR validation of 4 genes within the drug metabolism and protein synthesis category. In panels B & D, the expression levels of genes were normalized to *Gapdh* and/or *Arbp1/Rplp0* house-keeping genes. *$p < 0.05$, **$p < 0.01$, ***$p < 0.001$. (For interpretation of the references to color in this figure legend, the reader is referred to the web version of this article.)

activity is sufficient to regulate a subset of glutathione transferase genes (Fig. 3C). Indeed, while 5 isozymes were upregulated in TGL, a remarkable 8 *Gst* enzymes within the *alpha* and *mu* classes were increased in TGH hearts. The dose-dependent nature of *Gsta3* induction was validated in qPCR experiments as TGL exhibited 5–7-fold expression increases while TGH displayed 12–16-fold increases, respectively (Fig. 3D). Recently, we have reported that the levels of the reduced form of GSH and the ratio of reduced/oxidized glutathione (GSH/GSSG) were significantly altered. In particular, the ratio was increased (31.0 and 50.4 in TG-low and TG-high) in the hearts of TG vs. NTG (18.5) mice [16]. In addition to drug metabolism, IPA's disease annotation of glutathione metabolism included the biological category of protein synthesis (see Fig. 2B); therefore, DEGs presented in Fig. 3C also comprise this biological function. The ubiquitously expressed eukaryotic translation elongation factor 1 alpha 1 (*Eef1a1*) was elevated in the hearts of CaNrf2 mice (Fig. 3C). Intriguingly, this protein was recently shown to be required for the heat shock response as it facilitates *Hsp70*'s transcription, stabilization and nuclear export [24]. Dysregulated ELMO/CED-12 domain containing 1 (*Elmod1*), and tissue inhibitor of metalloproteinase 3 (*Timp3*) expression levels were validated in qPCR experiments. Similar to the reduced expression observed in human cardiomyopathy patients [25], *Timp3* mRNA was decreased by nearly 3-fold in TGH hearts (Fig. 3D). Consistent with the reports of exacerbated cardiac dysfunction due to enhanced matrix metalloproteinase (Mmp) activity in *Timp3* deficient mice [26], reduced *Timp3* expression in TGH mice was associated with concomitant increases in *Mmp2* and *Mmp10* expression (data not shown). Unexpectedly, the mean relative expression of the ARF family GTPase-activating protein [27] *Elmod1* dramatically increased to approximately 75 and 19-fold in TGH and TGL mice, respectively (Fig. 3D).

2.5. Exhausted stress response in CaNrf2-TG mice

CaNrf2 mediated disruptions in post-translational modification and cellular compromise functions were highlighted by disease annotations reflecting abnormal protein folding (see Fig. 2B). To this end, we discovered several heat shock genes severely compromised in RS hearts (Fig. 4A and C). Specifically, the co-chaperone FK506 binding proteins 4 and 5 (*Fkbp4*, *Fkbp5*), heat shock proteins 5, 8, 1, 1A, and 1B (*Hspa5*, *Hspa8*, *Hspb1*, *Hspa1a*, *Hspa1b*), DnaJ heat shock protein family

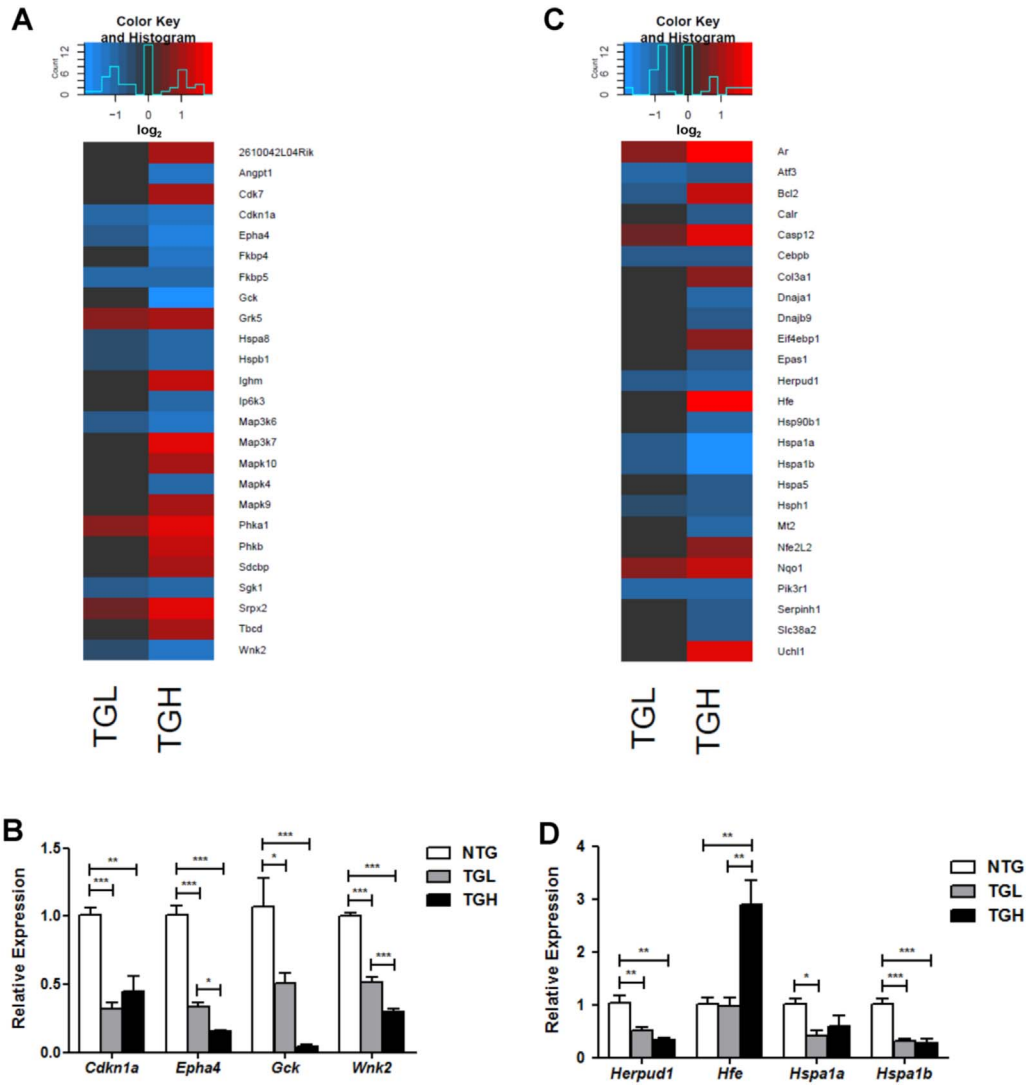

Fig. 4. Reduced chaperone expression in CaNrf2-TG mice. A) Heat map illustrating RNA sequencing log2 expression changes of the top 25 DEG's contained within IPA's biological function of post translational modifications. B) Real-time qPCR validation of 4 genes within the post translational modifications category. Heat map illustrating RNA sequencing log2 expression changes of the top 25 DEG's contained within IPA's biological function of cellular compromise. Real-time qPCR validation of 4 genes within the cellular compromise category. In panels B & D, the expression levels of genes were normalized to *Gapdh* and/or *Arbp1/Rplp0* house-keeping genes. *p < 0.05, **p < 0.01, ***p < 0.001.

Table 1
Decreased chaperone expression in CaNrf2 hearts.

Official gene symbol	HGNC official full name	TGL Log2-FC	TGH Log2-FC
Hspa8	heat shock protein family A (Hsp70) member 8	−0.62	−1.00
Hspa5	heat shock protein family A (Hsp70) member 5	NS	−0.89
Hspa1b	heat shock protein family A (Hsp70) member 1B	−0.89	−1.94
Hspa1a	heat shock protein family A (Hsp70) member 1A	−0.75	−1.80
Hspb1	heat shock protein family B (small) member 1	−0.60	−0.99
Hsp90b1	heat shock protein 90 beta family member 1	NS	−0.94
Hsp90aa1	heat shock protein 90 alpha family class A member 1	NS	−0.60
Hsp90ab1	heat shock protein 90 alpha family class B member 1	NS	−0.65
Hsph1	heat shock protein family H (Hsp110) member 1	−0.62	−0.82
Dnaja1	DnaJ heat shock protein family (Hsp40) member A1	NS	−0.91
Dnajb9	DnaJ heat shock protein family (Hsp40) member B9	NS	−0.72
Dnajb5	DnaJ heat shock protein family (Hsp40) member B5	NS	−1.03

Relative heat shock protein (Hsp) family gene expression in CaNrf2 TGL and TGH mice. Although the Hsp70 superfamily was primarily reduced in TGL mice, greater Nrf2 in TGH hearts was associated with a significant decrease in at least one member of each Hsp family. FC, fold-change; NS, not significant.

(Hsp40) members A1 and B9 (*Dnaja1*, *Dnajb9*), heat shock protein 90, beta (Grp94), member 1 (*Hsp90b1*), and the heat shock 105 kDa/110 kDa protein 1 (*Hsph1*) were all significantly downregulated in the TGH group (Fig. 4A and C). An extensive analysis of all TGH DEG's derived by RNAseq revealed significant decreases in 12 genes representing each major heat shock protein family [28] (Table 1). Interestingly, the heat shock response genes was not reduced as drastically as the Hsp70 superfamily members in TGL mice (Fig. 4E). Decreased *Hspa1a* and *Hspa1b* expressions were subsequently validated in qPCR experiments (Fig. 4D). In addition to the exhausted Hsp signature,

the expressions of calreticulin (*Calr*), homocysteine-inducible, endoplasmic reticulum stress-inducible, ubiquitin-like domain member 1 (*Herpud1*), and activating transcription factor 3 (*Atf3*) were suppressed in transgenic mouse hearts (Fig. 4C and D). The lack of stress response was accompanied by robust induction of caspase 12 (*Casp12*) in both TGL and TGH (Fig. 4C). Intriguingly, increased expression of the anti-apoptotic regulator B-cell leukemia/lymphoma 2 (*Bcl2*) [29] was observed, but the closely related BCL2-like 1 (*Bcl2l1*) was significantly reduced in both groups (Fig. 4C and data not shown). As a crucial modulator of calcium homeostasis in the endoplasmic reticulum, *Bcl2* expression changes in CaNrf2 mice may reflect a compensatory response to luminal ion flux rather than a survival response [20]. Indeed, significant decreases in the anti-apoptotic cyclin-dependent kinase inhibitor 1A (*Cdkn1a*) [30] were observed through real-time qPCR (Fig. 4B). Further validation of WNK lysine deficient protein kinase 2 (*Wnk2*), glucokinase (*Glk*), and EPH receptor A4 (*Epha4*) expression produced remarkable consistency with RNAseq results (Fig. 4B).

2.6. Cytoskeletal disarray and hindered striated muscle development and function

IPA analysis of CaNrf2 transcriptomes revealed enriched canonical actin signaling and perturbed biological functions related to cellular assembly and organization (see Fig. 2A and B). Diseases embodied by these functions were associated with cytoskeleton development, microtubule dynamics, and formation of actin filaments (see Fig. 2B). This is supported by the observed decrease in centromere protein F (*Cenpf*) expression in TGH mice (Fig. 5A), whose loss of function in the heart produces cardiomyopathy and microtubule disarray [31]. Furthermore, TGH mice exhibited significant decreases in actin-binding LIM protein 1 (*Ablim1*) and filamin binding LIM protein 1 (*Fblim1*) (Fig. 5A). Conversely, the microtubule associated protein 1a (*Map1a*) was robustly induced in both transgenic groups while microtubule-associated protein 1b (*Mapb1b*) expression was significantly increased only in TGH (Fig. 5A). Real-time qPCR validation of *Map1a* expression revealed 15 and 18-fold increases in TGL and TGH, respectively (Fig. 5B). An important mediator of myotubularin protein stability, myotubularin related protein 12 (*Mtmr12*) mRNA was increased in TGH mice (Fig. 5A) suggesting deficits in intermediate filament organization [32]. Validation of decreased laminin, alpha 5 (*Lama5*) and ephrin B3 (*Efnb3*) expression were consistent with RNAseq data (Fig. 5B). Decreased *Efnb3* expression in the RS model may contribute to cardiac dysfunction as the deletion of this actin regulator enhances contractility of vascular smooth muscle cells [33]. Reticulon 4 (*Rtn4*) expression was dose-dependently increased to approximately 2 and 3-fold in CaNrf2 TGL and TGH group, respectively (Fig. 5B). This may reflect a compensatory response to the pronounced chaperone depletion in TGH mice as particular *Rtn4* isoforms have been shown to orchestrate chaperone distribution [34].

Alterations in the cytoskeletal transcriptional profile persisted with genes involved in striated muscle development and function (Fig. 5C). The co-expressed skeletal and cardiac sarcomeric alpha actin isoforms *Acta1* and *Actc1*, respectively, were significantly dysregulated in CaNrf2 mice [35]. However, TGL and TGH groups displayed distinct patterns of expression as *Acta1* mRNA was increased in TGL but markedly decreased in TGH (Fig. 5C), and *Actc1* expression increased only in TGH (data not shown). The variation in *Acta1* expression between genotypes was confirmed by qPCR (Fig. 5D). Despite differences in skeletal and cardiac actin expression, both groups displayed robust induction of actin, alpha 2, smooth muscle, and aorta (*Acta2*) (Fig. 5C). In line with reports of *Acta2* induction in myofibroblast transition, the greater expression of this actin isoform in TGH mice coincided with significant increases in 6 collagen-related genes unchanged in TGL mice; *Col4a5*, *Col3a1*, *Col1a1*, *Col22a1*, *Col15a1*, and *Colq* (data not shown) [36]. Disturbances in the TGH contractile apparatus are likely as significant decreases were observed in the expression of myotilin (*Myot*), myomesin 2 (*Myom2*), myosin binding protein C, fast type (*Mybpc2*), tropomyosin 4 (*Tpm4*), and sodium channel, voltage-gated, type IV, alpha (*Scn4a*). Interestingly, none of these genes were dysregulated in the TGL group (Fig. 5C) suggesting dose-dependent effects of Nrf2 activity on structural disorganization of the myocardium. Further, myosin, light chain 1 (*Myl1*) expression was increased in only the TGH group as a 3-fold induction was detected in qPCR validation experiments (Fig. 5D). In addition to expression patterns implying altered sarcomere architecture, the expression of ankyrin repeat domain 1 (*Ankrd1*), a cardiac transcriptional regulator commonly increased in human heart failure patients was found to be increased nearly 3-fold and 5-fold in TGL and TGH groups, respectively (Fig. 5D) [37]. Importantly, *Ankrd1* stimulation of cardiac fetal programs is implicated in cardiomyocyte hypertrophy as a loss of function abrogates α-adrenergic mediated growth [38]. Lastly, Glucan (1,4-alpha-), branching enzyme 1 (*Gbe1*), a hypoxia-sensitive enzyme involved in glycogen biogenesis [39], was dose-dependently increased according to the level of CaNrf2 transgene (Fig. 5D). The 3-fold increase in relative *Gbe1* expression seen in TGH hearts is consistent with the robust induction of canonical eNOS and cardiovascular hypoxia signaling pathways observed in this group (see Fig. 2A).

2.7. Aberrant antioxidant signaling and impaired protein quality control in RS hearts

Both CaNrf2 groups revealed significant increases in the expression of hypertrophic genes natriuretic peptides A and B (*Nppa*, *Nppb*) (Fig. 6A and C). Interestingly, TGH mice revealed significant down-regulation in several myosin heavy chain isoforms including *Myh6*, *Myh4*, *Myh9* and *Myh1*; however, no significant changes were detected for these genes in TGL hearts (Fig. 6A and data not shown). Moreover, Kruppel like factor 15 (*Klf15*), a negative regulator of cardiac hypertrophy whose deficiency is associated with heart failure, was significantly decreased only in TGH (Fig. 6B) [40,41]. In line with the transcriptional dysregulation of excitation-contraction coupling genes described previously (see Fig. 5A and C), a robust effect of Nrf2 activity on bridging integrator 1 (*Bin1*) expression was observed (Fig. 6A and B). As a facilitator of t-tubule biogenesis and mediator of their interaction with L-type calcium channels, the *Bin1*-microtubule scaffolding complex plays pivotal roles in calcium regulation during cardiomyocyte contraction [42–44]. Mean *Bin1* expression increased 8-fold in TGL and 13-fold in TGH groups, respectively (Fig. 6B). Further, the expression of calreticulin 3 (*Calr3*) increased 2 and 3-fold in TGL and TGH groups, respectively, highlighting another potential link between calcium perturbations and contraction in the CaNrf2 model [45] (Fig. 6D). In addition to the increased *Myl1* transcription previously described (see Fig. 5D), both CaNrf2 groups exhibited significant upregulation in myosin, light chain 4 (*Myl4*) expression, with 7 and 29-fold increases detected in TGL and TGH mRNA, respectively (Fig. 6B). Ectopic phospholipase A2, group VII (*Pla2g7*) expression was also identified in the RS model as TGL and TGH hearts demonstrated nearly 10 and 14-fold increases in relative mRNA levels (Fig. 6C and D). Intriguingly, *Pla2g7* has been shown to be a transcriptional target of Nrf3 and polymorphisms as well as its expression levels have been implicated in coronary artery disease and atherosclerosis progression [46–48].

Consistent with diminished *Timp3* mRNA levels previously described (See Fig. 3D), tissue inhibitor of metalloproteinase 4 (*Timp4*) expression was also significantly decreased in CaNrf2 mice (Fig. 6B). Importantly, *Timp4* loss of function results in reduced cardiac function with age and increased susceptibility to myocardial infarction [49], a biological process found to be over-represented in CaNrf2 IPA experiments (see Fig. 2B). Moreover, mechanisms of myocardial cell death were found to be enriched in the transgenic hearts (see Fig. 2A and B). Pannexin 1 (*Panx1*), a cardiomyocyte cation channel previously reported to facilitate apoptotic signaling [50,51], was robustly upregulated in a dose-dependent fashion with TGL and TGH mice exhibiting nearly 9 and 17-fold increases (Fig. 6D). Death associated protein (*Dap*), a facilitator of JNK-mediated apoptosis [52], also increased according

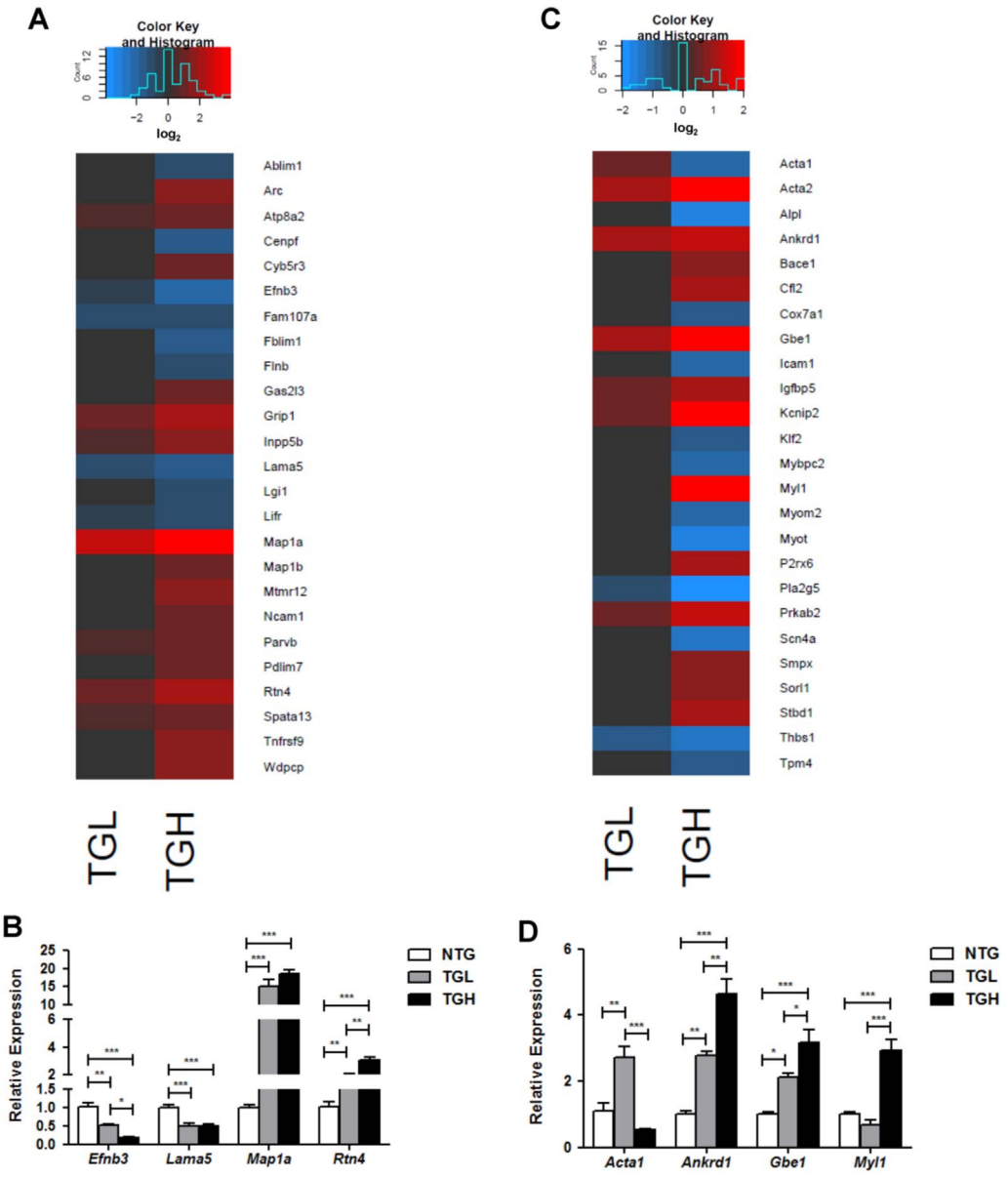

Fig. 5. Cytoskeletal disarray and hindered striated muscle development and function. A) Heat map illustrating RNA sequencing log2 expression changes of the top 25 DEG's contained within IPA's biological function of cellular assembly and organization. Real-time qPCR validation of 4 genes within the cellular assembly and organization category. Heat map illustrating RNA sequencing log2 expression changes of the top 25 DEG's contained within IPA's biological function of skeletal and muscular development and function. D) Real-time qPCR validation of 4 genes within the skeletal and muscular development and function category. In panels B & D, the expression levels of genes were normalized to *Gapdh* and/or *Arbp1/Rplp0* house-keeping genes. *p < 0.05, **p < 0.01, ***p < 0.001.

to the level of Nrf2 with 5-fold and 10-fold increases observed in TGL and TGH groups, respectively (Fig. 6F). Previous observations of Hsp27 interacting with Dap to prevent apoptosis suggests that cell death may occur downstream of chaperone depletion in the CaNrf2 model of cardiac RS [53]. In further support of myocyte death, Myeloid/lymphoid or mixed-lineage leukemia; translocated to, 11 (*Mllt11*), an inducer of Bad-mediated intrinsic apoptosis, was also found to be significantly upregulated by approximately 3-fold in both groups (Fig. 6F) [54]. Moreover, the TNF-alpha induced protein 8 (*Tnfaip8*), which can inhibit caspase activity, was significantly reduced in the TGH group (Fig. 6F) [55]. Notably, this expression pattern was observed in the presence of dramatic induction of the Nrf2 antioxidant target sulfiredoxin 1 (*Srxn1*) [56]. Despite 5 and 14-fold increases in the relative expression of *Srxn1* coupled with the robust pro-survival antioxidant profile previously described (see Figs. 2 and 3), TGL and TGH groups displayed a transcriptional signature reflecting cardiomyocyte death and concomitant cardiovascular pathology (Fig. 7).

3. Discussion

Nrf2 mediated induction of ARE and EpRE gene expression is a critical response for cellular defense against free radical damage and oxidative stress [57]. Recent reports have illuminated roles for Nrf2 distinct from canonical redox signaling, whereby key players in the unfolded protein response (UPR) serve as both upstream stimulators [9] as well as downstream targets of Nrf2 signaling [10]. Our previous work implicated aberrant Nrf2 activity in the hR120G αB-Crystallin model of mutant protein aggregation cardiomyopathy (MPAC) [11–13] and demonstrated a rescue of cardiac function in MPAC mice upon normalization of Nrf2 [11]. Many studies reveal that induction of antioxidant and cytoprotective genes could be of potential therapeutic benefits, but there is a lack of clinically relevant animal models of chronic antioxidant function that can not only improve our understanding of the role of antioxidants in the pathogenesis of cardiac diseases but also evaluate the therapeutic potential and risks of their sustained bio-availability and/or activation. Thus, in the current study, we have used the CaNrf2 transgenic mouse model with cardiac-specific constitutive Nrf2 nuclear translocation to explore the transcriptional signature of cardiac reductive stress (RS) directly by modulating the antioxidant transcription factor Nrf2 without altering any other redox-sensitizing backgrounds such as αB-Crystallin mutation. Transcriptome analysis of low (TGL) and high (TGH) transgene expressing mice

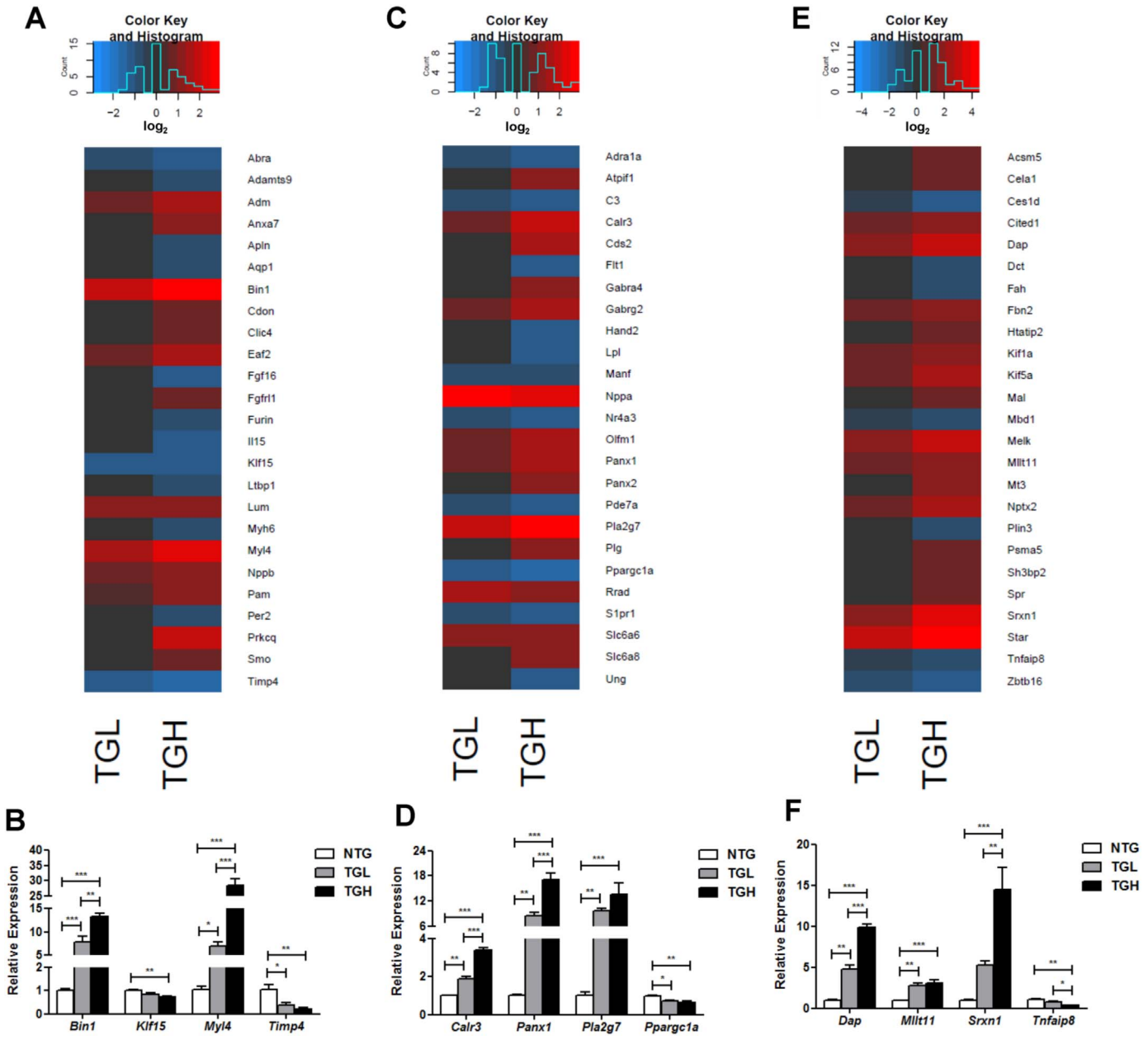

Fig. 6. Aberrant antioxidant signaling and impaired protein quality control in RS hearts. A) Heat map illustrating RNA sequencing log2 expression changes of the top 25 DEG's contained within IPA's biological function of cardiovascular system development and function. B) Real-time qPCR validation of 4 genes within the cardiovascular system development and function. C) Heat map illustrating RNA sequencing log2 expression changes of the top 25 DEG's contained within IPA's biological function of cardiovascular disease. D) Real-time qPCR validation of 4 genes within the cardiovascular disease category. E) Heat map illustrating RNA sequencing log2 expression changes of the top 25 DEG's contained within IPA's biological function of cell death. F) Real-time qPCR validation of 4 genes within the cell death category. In panels B, D, & F, the expression levels of genes were normalized to *Gapdh* and/or *Arbp1/Rplp0* housekeeping genes. *$p < 0.05$, **$p < 0.01$, ***$p < 0.001$.

revealed a dose-dependent role for Nrf2 (gain of function) in potentiating varying degrees of a reductive-redox signature in the myocardium. More importantly, as the multifaceted roles for Nrf2 signal transduction are becoming increasingly apparent, these genetic tools will allow investigators to shed light on the appropriate range for Nrf2 activity in promoting redox equilibrium during physiological vs. pathological processes.

Constitutively active Nrf2 in TG mouse hearts generated a robust induction of numerous antioxidant and glutathione metabolizing genes. To this end, significant increases in *Cat*, *Gclm*, *Gpx1*, *Gpx3*, *Gss*, *Gsr*, *Heph*, *Nqo1*, *Prdx6*, *Srxn1, Txn1*, and *Txnrd1* expression were detected. Moreover, dramatic increases in multiple isozymes within each of the alpha and mu classes of the glutathione s-transferase family were observed. These detoxifying enzymes play significant regulatory roles in signal transduction through s-glutathionylation of electrophilic cysteine residues [58]. Therefore, while initial glutathione s-transferase expression may help restore homeostasis during an oxidative insult, sustained increases in reducing equivalents and aberrant s-glutathionylation likely augments RS through ectopic mixed disulfide bond formation. If this phenomenon is indeed at play during hyperactive Nrf2 signaling, the failed heat shock response observed in CaNrf2 hearts would certainly exacerbate protein folding impairments. Strikingly, constitutive activation of Nrf2 transcriptional programs decreased the expression of at least one member in each of the major heat shock protein families as well as co-chaperones and protein disulfide isomerase (PDI) associated genes. Undoubtedly, this expression profile reflects a failure to meet the demands of protein folding machinery. Paradoxically, chaperones have been cited as Nrf2 target genes and this

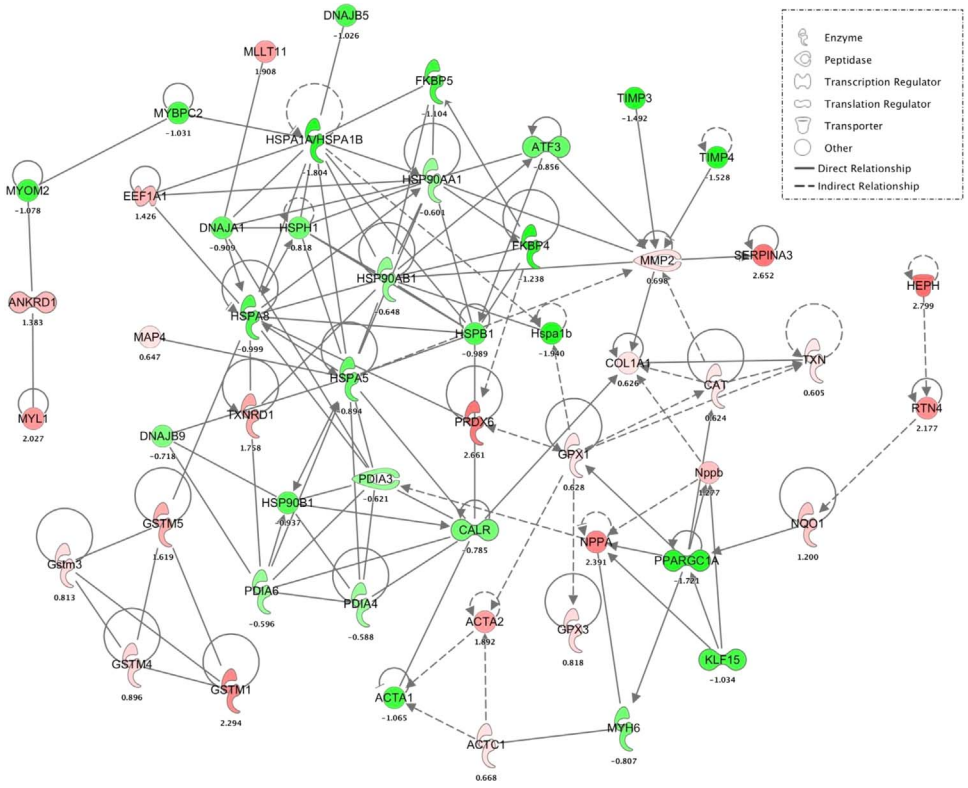

Fig. 7. Cardiac reductive stress gene network. Each circle represents individual gene. The solid line indicates direct and dotted lines indicate indirect genetic interactions encompassed by the major biological alterations seen in the CaNrf2 model. Different classes of genes are represented by different color and shape as indicated the figure key. (For interpretation of the references to color in this figure legend, the reader is referred to the web version of this article.)

mechanism has been reported to promote survival upon cellular stress [1]. However, much like the necessity for balance in *Gst* activity and other redox-dependent reactions, we speculate that Nrf2 transcriptional responses are double-edged whereby acute induction enhances protein quality control mechanisms but chronic activity promotes proteotoxicity [12]. Indeed, this notion is supported by a CaNrf2 expression pattern lacking genes critical for UPR resolution, but enhanced induction of the endoplasmic reticulum stress-sensitive caspase *Casp12* [59].

As a crucial organelle involved in calcium homeostasis [60], ER perturbations upon sustained activation of Nrf2 gene programs have remarkable implications for cardiac function. Proper maintenance of calcium is a prerequisite for excitation-contraction coupling, and numerous investigations have highlighted the relevance for abnormal calcium handling in hypertrophy and heart failure [61]. In CaNrf2 mice, sustained Nrf2 activity dose-dependently dysregulated canonical calcium signaling and increased the expression of the sarcoplasmic reticulum calcium chaperone *Calr3* (*Fig. 7*). Furthermore, the transcriptional activation of *Rtn4* (Nogo) may reflect remodeling of the reticular network in the CaNrf2 model [62,63]. Similarly, the striking induction of *Bin1* expression is suggestive of alterations in the physical interaction between t-tubules and L-type calcium channels, two structures which are vital to cardiomyocyte contraction [42].

Cytoskeletal disarray observed in the CaNrf2 myocardium likely compounds altered calcium dynamics to collectively dysregulate the contractile apparatus during cardiac RS. In this regard, a battery of sarcomeric genes were repressed in TGH mice including *Mybpc2*, *Myh4*, *Myh6*, *Myh1*, *Myh9*, *Myom2*, *Myot*, and *Tpm4*. Importantly, the actin cytoskeleton is an active site for s-glutathionylation, and this post-translational modification has been reported to repress actin polymerization rates [64]. Furthermore, s-glutathionylation mediated decrements in actin polymerization following ischemia hinder contractile force production [65]. Therefore, Nrf2 mediated RS may disrupt integral actin interactions required for physiological contraction. Accordingly, the observed increase in cardiac actin expression (*Actc1*) may represent a compensatory response to restore cytoskeletal integrity.

In addition to expression patterns reflecting altered contractility, the CaNrf2 transcriptome revealed marked increases in several markers of hypertrophy and cardiovascular disease. Along these lines, Nrf2 levels in low and high transgene expressing CaNrf2 mice dose-dependently enhanced *Ankrd1* expression. This stretch-sensitive transcriptional co-factor has been well characterized to be upregulated in heart failure [37]. Ankrd1 participates in a signaling complex with the cardiogenic transcription factor Gata4 to facilitate its nuclear translocation and enhance hypertrophic gene expression [38]. Diminished *Klf15* expression in CaNrf2 mice may exacerbate this mechanism as it has been previously shown to repress Gata4 activity [40]. While Klf15 deficiency coincides with murine and human heart failure [41], its overexpression in cardiomyocytes reduces *Nppa* mRNA levels [40]. Since the *Nppa* expression was dramatically induced with increasing levels of the CaNrf2 transgene, there is a strong likelihood that *Ankrd1/Klf15/Gata4* dysregulation may underlie cardiovascular pathophysiology in Nrf2 mediated RS.

Interestingly, *Klf15* has also been reported to negatively regulate myocardial fibrosis as hypertrophied hearts from *Klf15*$^{-/-}$ mice display excessive collagen deposition [66]. Accordingly, the diminished *Klf15* expression in CaNrf2 TGH mice was accompanied by an upregulation in a several collagen-related genes. Additionally, the Klf15 depleted CaNrf2 myocardium displayed robust induction of the myofibroblast marker *Acta2*, a downstream target of the pro-fibrotic TGFβ1 cascade which has been reported to be suppressed by *Klf15* activity [36,66]. TGFβ1 mediated myofibroblast accumulation has also been reported to disrupt the equilibrium between matrix metalloproteinases (Mmps) and their inhibitors (Timps) [36], thus diminished *Timp3* and *Timp4* expression with simultaneous increases in *Mmp2* and *Mmp10* lends further support the notion of potential fibrotic remodeling in cardiac RS. Since enhanced TGFβ1 activity and fibrosis accompany the progression from human cardiac hypertrophy to heart failure [67], the fibrotic expression profile in the CaNrf2 model may provide insight into the redox dependent relationships involved in this process (Fig. 7).

Future investigations employing the CaNrf2 model should aim to examine if hyperactive Ire1α autophosphorylation facilitates endoplasmic reticulum (ER) associated death cascades as this canonical

UPR moderator has been shown to promote JNK mediated cell death upon sustained ER dysfunction [68]. The decay of chaperone mRNA, which was remarkably observed in our transcriptional analyses, indicates a significant impairment of protein folding repair pathways. Interestingly, Hsp27 has been shown to prevent cell death by interacting with Dap, an upstream activator of JNK [52,53]. Therefore, the dose-dependent increases in *Dap* expression with concomitant repression of UPR genes expression may reflect Ire1α mediated ER apoptotic signaling through JNK in our model of cardiac RS. A more recent investigation of the hyperactive Ire1α mechanism described the requirement for thioredoxin-interacting protein (*Txnip*) in facilitating cell death during ER stress [69]. Although RNA sequencing did not reveal altered *Txnip* expression, thioredoxin 1 (*Txn1*) and thioredoxin reductase 1 (*Txnrd1*) were upregulated in TG mice with RS.

In summary, constitutive Nrf2 signaling in the novel CaNrf2-TG model revealed a transcriptional signature suggestive of dose-dependent reductive-redox (i.e. Pro-reductive or RS conditions). Given our previous findings that CaNrf2-TG mice developed hyper-reductive state (increased glutathione and GSH/GSSG redox state) at 10–12 weeks of age, it is likely that these mice may exhibit chronic reductive stresses, which then lead to pathological cardiac remodeling. As it is inappropriate to make mechanistic claims from complex expression data, future experiments will exploit this genetic tool to elucidate underappreciated roles for aberrant antioxidant responses in disrupting various pathways including organelle redox homeostasis, protein folding, cardiac remodeling, muscle development and cell death.

4. Methods

4.1. Animals

Heart-specific constitutively active Nrf2 (CaNrf2) transgenic mouse lines (TG-low and TG-high) were utilized as described in our recent publication [16]. Briefly, the transgenic mice expressing constitutively active form of Nrf2 was generated using a construct that lacked a functional Neh2 domain responsible for Keap1 repression under the control of alpha-myosin heavy chain (α-MHC) promoter allowing the expression of Nrf2 only in the myocardium. Based on the levels of transgene expression, the founder lines #9384 and #1531 were designated as TG-low and TG-high, respectively. The founder lines and breeding colonies were maintained distinctly [16]. All mice were housed and maintained under controlled conditions in the animal research facility at the University of Utah or the University of Alabama at Birmingham. Each cage housed not more than five mice and all mice had free access to food (standard rodent diet) with water ad libitum. All animal experimental procedures were approved by the Institutional Animal Care and Use Committee (IACUC) of the University of Utah and the University of Alabama at Birmingham.

4.2. Next generation RNA sequencing

RNA was isolated from 6 to 8 month male NTG and CaNrf2 (Low and High) mouse hearts (n = 3–4/group) using the RNeasy Mini Kit (Qiagen, Cat. 74106) according to the manufacturer's instructions. The purity of RNA was confirmed using Bio-analyzer and intact poly(A) transcripts were purified from total RNA using oligo(dT) magnetic beads and mRNA sequencing libraries were prepared with the TruSeq Stranded mRNA Library Preparation Kit (Illumina, RS-122-2101, RS-122-2102). A D1000 ScreenTape assay (Agilent, Cat. 5067-5582/3) was used with the 2200 TapeStation Instrument (Agilent Technologies) to qualify purified libraries. The cBot was used to apply 18pM of the sequencing library to a TruSeq v3 flowcell (Illumina) and the TruSeq SR Cluster Kit (Illumina, Cat. GD-401-3001) was used for clonal amplification. Finally, the flowcell was transferred to the HiSeq. 2000 instrument and used in 50 cycle single read sequence run performed with TruSeq SBS Kit v3-HS reagents (Illumina, Cat. FC-401-3002). Novoindex (2.8) was used to create a reference index on a combination of the hg19 chromosome and splice junction sequences. Splice junction sequences were generated with USeq (v8.6.4) MakeTranscriptome using Ensembl transcript annotations (build 67). Reads were aligned to the transcriptome reference index described above using Novoalign (v2.08.01), allowing up to 50 alignments for each read. USeq's SamTranscriptomeParser application was used to select the best alignment for each read and convert the coordinates of reads aligning to splices back to genomic space. Differential gene expression was measured using USeq's DefinedRegionDifferentialSeq application. The number of reads aligned to each gene was calculated. The counts were then used in DESeq (v1.24.0), which normalizes the signal and determines differential expression.

4.3. Ingenuity pathway analysis

Following RNAseq analysis, all differentially expressed genes (DEGs) in TGL and TGH groups were subjected to Ingenuity Pathway Analysis (IPA) (Qiagen). Two separate IPA runs were conducted for TGL and TGH groups relative to the NTG expression profile. Log-transformed p-values of significantly enriched canonical pathways associated with the cardiac reductive stress transcriptome were used to construct a heat map. In addition to canonical pathways, IPA data output provided significantly altered biological functions with corresponding disease annotations, and p-values were again transformed to configure a heat map representing the major biological perturbations in the CaNrf2 reductive stress model. IPA analysis included gene lists for each disease annotation, and the top 25 DEGs in CaNrf2 mice within each major biological function category were assembled into heat maps based on their $\log_2$ relative expression ratios.

4.4. RNA isolation and real-time qPCR validation

Approximately 10–25 mg heart tissue stored in RNAlater stabilization solution was used for RNA extraction using the RNeasy kit (Qiagen). Following isolation, the RNA was quantified and assessed for purity with a NanoDrop Spectrophotometer (ThermoFisher Scientific). 1–1.25 μg RNA was reverse transcribed to synthesize cDNA using the QuantiTect Kit (Qiagen) according to the manufacturer's instructions. QuantiTect SYBR Green PCR kits (Qiagen) were used to perform 10 μl real-time qPCR reactions with 30–37.5 ng cDNA template and 1pmol of respective primer sets (refer Supplementary material Table 1) and was amplified by a Roche LightCycler 480 (Roche Life Science). Copy numbers of cDNA targets were quantified using Ct values, and mRNA fold changes were calculated by normalization to the Ct of housekeeping genes *Arbp1* or *Gapdh* according to the $2^{-\Delta\Delta Ct}$ method. 4 genes within each IPA biological function category were validated using 4–6 animals per group to compare expression differences between CaNrf2 and NTG genotypes at 6–8 months of age.

4.5. Statistics

Fold changes in gene expression were calculated according to the $2^{-\Delta\Delta Ct}$ method and data are presented as mean ± SEM (n = 4–6/group). Basal comparisons between NTG vs. CaNrf2-TG (low or high) mice were made using a one-way analysis of variance (ANOVA) with Tukey's post-hoc. All statistical analyses were performed using GraphPad Prism-7 software with significance set at $p < 0.05$.

Acknowledgements

This study was supported by funding from NHLBI (HL118067), NIA (AG042860), the AHA (BGIA 0865015F), the Division of Cardiovascular Medicine/Department of Medicine, University of Utah and the start-up funds (3115851.000.213115851.392300000.0000 for NSR) by Departments of Pathology and Medicine, the University of Alabama at

Birmingham, AL.

The authors would like to thank Dr. Brian Dalley, High-Throughput Genomics and Bioinformatic Analysis Shared Resource of the Huntsman Cancer Institute at the University of Utah for their assistance with RNA sequencing experiments and data analyses. Authors' also thank Ms. Jennifer Hong and Ms. Nancy Atieno for their assistance in maintaining the animal colonies and Mrs. Jennifer Schroff for editorial assistance.

Appendix A. Supplementary material

Supplementary data associated with this article can be found in the online version at http://dx.doi.org/10.1016/j.redox.2017.07.013.

References

[1] T.W. Kensler, N. Wakabayashi, S. Biswal, Cell survival responses to environmental stresses via the Keap1-Nrf2-ARE pathway, Annu. Rev. Pharmacol. Toxicol. 47 (2007) 89–116.
[2] K. Itoh, N. Wakabayashi, Y. Katoh, T. Ishii, K. Igarashi, J.D. Engel, M. Yamamoto, Keap1 represses nuclear activation of antioxidant responsive elements by Nrf2 through binding to the amino-terminal Neh2 domain, Genes Dev. 13 (1999) 76–86.
[3] M.-I. Kang, A. Kobayashi, N. Wakabayashi, S.-G. Kim, M. Yamamoto, Scaffolding of Keap1 to the actin cytoskeleton controls the function of Nrf2 as key regulator of cytoprotective phase 2 genes, Proc. Natl. Acad. Sci. 101 (2004) 2046–2051.
[4] M. McMahon, K. Itoh, M. Yamamoto, J.D. Hayes, Keap1-dependent proteasomal degradation of transcription factor Nrf2 contributes to the negative regulation of antioxidant response element-driven gene expression, J. Biol. Chem. 278 (2003) 21592–21600.
[5] D.D. Zhang, M. Hannink, Distinct cysteine residues in Keap1 are required for Keap1-dependent ubiquitination of Nrf2 and for stabilization of Nrf2 by chemopreventive agents and oxidative stress, Mol. Cell. Biol. 23 (2003) 8137–8151.
[6] M. Komatsu, H. Kurokawa, S. Waguri, K. Taguchi, A. Kobayashi, Y. Ichimura, Y.-S. Sou, I. Ueno, A. Sakamoto, K.I. Tong, The selective autophagy substrate p62 activates the stress responsive transcription factor Nrf2 through inactivation of Keap1, Nat. Cell Biol. 12 (2010) 213–223.
[7] Y.-C. Yang, C.-K. Lii, A.-H. Lin, Y.-W. Yeh, H.-T. Yao, C.-C. Li, K.-L. Liu, H.-W. Chen, Induction of glutathione synthesis and heme oxygenase 1 by the flavonoids butein and phloretin is mediated through the ERK/Nrf2 pathway and protects against oxidative stress, Free Radic. Biol. Med. 51 (2011) 2073–2081.
[8] E.-J. Joung, M.-H. Li, H.G. Lee, N. Somparn, Y.S. Jung, H.-K. Na, S.-H. Kim, Y.-N. Cha, Y.-J. Surh, Capsaicin induces heme oxygenase-1 expression in HepG2 cells via activation of PI3K-Nrf2 signaling: NAD (P) H: quinone oxidoreductase as a potential target, Antioxid. Redox Signal. 9 (2007) 2087–2098.
[9] S.B. Cullinan, J.A. Diehl, PERK-dependent activation of Nrf2 contributes to redox homeostasis and cell survival following endoplasmic reticulum stress, J. Biol. Chem. 279 (2004) 20108–20117.
[10] K.M. Glover-Cutter, S. Lin, T.K. Blackwell, Integration of the unfolded protein and oxidative stress responses through SKN-1/Nrf, PLoS Genet. 9 (2013) e1003701.
[11] S. Kannan, V.R. Muthusamy, K.J. Whitehead, L. Wang, A.V. Gomes, S.E. Litwin, T.W. Kensler, E.D. Abel, J.R. Hoidal, N.S. Rajasekaran, Nrf2 deficiency prevents reductive stress-induced hypertrophic cardiomyopathy, Cardiovasc. Res. (2013) cvt150.
[12] N.S. Rajasekaran, S. Varadharaj, G.D. Khanderao, C.J. Davidson, S. Kannan, M.A. Firpo, J.L. Zweier, I.J. Benjamin, Sustained activation of nuclear erythroid 2-related factor 2/antioxidant response element signaling promotes reductive stress in the human mutant protein aggregation cardiomyopathy in mice, Antioxid. Redox Signal. 14 (2011) 957–971.
[13] A.C. Brewer, S.B. Mustafi, T.V. Murray, N.S. Rajasekaran, I.J. Benjamin, Reductive stress linked to small HSPs, G6PD, and Nrf2 pathways in heart disease, Antioxid. Redox Signal. 18 (2013) 1114–1127.
[14] W. Dröge, Free radicals in the physiological control of cell function, Physiol. Rev. 82 (2002) 47–95.
[15] K.K. Griendling, D. Sorescu, B. Lassègue, M. Ushio-Fukai, Modulation of protein kinase activity and gene expression by reactive oxygen species and their role in vascular physiology and pathophysiology, Arterioscler. Thromb. Vasc. Biol. 20 (2000) 2175–2183.
[16] G. Shanmugam, M. Narasimhan, S. Tamowski, V. Darley-Usmar, N.S. Rajasekaran, Constitutive activation of Nrf2 induces a stable reductive state in the mouse myocardium, Redox Biol. (2017).
[17] S. Briancon, S. Boini, S. Bertrais, F. Guillemin, P. Galan, S. Hercberg, Long-term antioxidant supplementation has no effect on health-related quality of life: the randomized, double-blind, placebo-controlled, primary prevention SU.VI.MAX trial, Int. J. Epidemiol. 40 (2011) 1605–1616.
[18] P.M. Kris-Etherton, A.H. Lichtenstein, B.V. Howard, D. Steinberg, J.L. Witztum, Antioxidant vitamin supplements and cardiovascular disease, Circulation 110 (2004) 637–641.
[19] H. Lu, P.W. Fedak, X. Dai, C. Du, Y.-Q. Zhou, M. Henkelman, P.S. Mongroo, A. Lau, H. Yamabi, A. Hinek, Integrin-linked kinase expression is elevated in human cardiac hypertrophy and induces hypertrophy in transgenic mice, Circulation 114 (2006) 2271–2279.
[20] P. Pinton, R. Rizzuto, Bcl-2 and Ca2+ homeostasis in the endoplasmic reticulum, Cell Death Differ. 13 (2006) 1409–1418.
[21] S. Hein, S. Kostin, A. Heling, Y. Maeno, J. Schaper, The role of the cytoskeleton in heart failure, Cardiovasc. Res. 45 (2000) 273–278.
[22] J. Yang, B. Maity, J. Huang, Z. Gao, A. Stewart, R.M. Weiss, M.E. Anderson, R.A. Fisher, Regulator of G protein signaling 6 (RGS6) mediates doxorubicin-induced myocardial cell apoptosis and cardiomyopathy, FASEB J. 27 (2013) (1031.1037-1031.1037).
[23] J. Yang, B. Maity, J. Huang, Z. Gao, A. Stewart, R.M. Weiss, M.E. Anderson, R.A. Fisher, G-protein inactivator RGS6 mediates myocardial cell apoptosis and cardiomyopathy caused by doxorubicin, Cancer Res. 73 (2013) 1662–1667.
[24] M. Vera, B. Pani, L.A. Griffiths, C. Muchardt, C.M. Abbott, R.H. Singer, E. Nudler, The translation elongation factor eEF1A1 couples transcription to translation during heat shock response, Elife 3 (2014) e03164.
[25] Y.Y. Li, A.M. Feldman, Y. Sun, C.F. McTiernan, Differential expression of tissue inhibitors of metalloproteinases in the failing human heart, Circulation 98 (1998) 1728–1734.
[26] V. Kandalam, R. Basu, T. Abraham, X. Wang, A. Awad, W. Wang, G.D. Lopaschuk, N. Maeda, G.Y. Oudit, Z. Kassiri, Early activation of matrix metalloproteinases underlies the exacerbated systolic and diastolic dysfunction in mice lacking TIMP3 following myocardial infarction, Am. J. Physiol.-Heart Circ. Physiol. 299 (2010) H1012–H1023.
[27] A.A. Ivanova, M.P. East, L.Y. Slee, R.A. Kahn, Characterization of recombinant ELMOD (cell engulfment and motility domain) proteins as GTPase-activating proteins (GAPs) for ARF family GTPases, J. Biol. Chem. 289 (2014) 11111–11121.
[28] H.H. Kampinga, J. Hageman, M.J. Vos, H. Kubota, R.M. Tanguay, E.A. Bruford, M.E. Cheetham, B. Chen, L.E. Hightower, Guidelines for the nomenclature of the human heat shock proteins, Cell Stress Chaperones 14 (2009) 105–111.
[29] G. Kroemer, The proto-oncogene Bcl-2 and its role in regulating apoptosis, Nat. Med. 3 (1997) 614–620.
[30] O. Cazzalini, A.I. Scovassi, M. Savio, L.A. Stivala, E. Prosperi, Multiple roles of the cell cycle inhibitor p21 CDKN1A in the DNA damage response, Mutat. Res./Rev. Mutat. Res. 704 (2010) 12–20.
[31] E. Dees, P.M. Miller, K.L. Moynihan, R.D. Pooley, R.P. Hunt, C.L. Galindo, J.N. Rottman, D.M. Bader, Cardiac-specific deletion of the microtubule-binding protein CENP-F causes dilated cardiomyopathy, Dis. Models Mech. 5 (2012) 468–480.
[32] K. Hnia, H. Tronchère, K.K. Tomczak, L. Amoasii, P. Schultz, A.H. Beggs, B. Payrastre, J.L. Mandel, J. Laporte, Myotubularin controls desmin intermediate filament architecture and mitochondrial dynamics in human and mouse skeletal muscle, J. Clin. Investig. 121 (2011) 70–85.
[33] Y. Wang, Z. Wu, E. Thorin, J. Tremblay, J.L. Lavoie, H. Luo, J. Peng, S. Qi, T. Wu, F. Chen, Estrogen and testosterone in concert with EFNB3 regulate vascular smooth muscle cell contractility and blood pressure, Am. J. Physiol.-Heart Circ. Physiol. 310 (2016) H861–H872.
[34] Y.S. Yang, N.Y. Harel, S.M. Strittmatter, Reticulon-4A (Nogo-A) redistributes protein disulfide isomerase to protect mice from SOD1-dependent amyotrophic lateral sclerosis, J. Neurosci. 29 (2009) 13850–13859.
[35] D. Tondeleir, D. Vandamme, J. Vandekerckhove, C. Ampe, A. Lambrechts, Actin isoform expression patterns during mammalian development and in pathology: insights from mouse models, Cell Motil. Cytoskelet. 66 (2009) 798–815.
[36] B.C. Berk, K. Fujiwara, S. Lehoux, ECM remodeling in hypertensive heart disease, J. Clin. Investig. 117 (2007) 568–575.
[37] O. Zolk, M. Frohme, A. Maurer, F.-W. Kluxen, B. Hentsch, D. Zubakov, J.D. Hoheisel, I.H. Zucker, S. Pepe, T. Eschenhagen, Cardiac ankyrin repeat protein, a negative regulator of cardiac gene expression, is augmented in human heart failure, Biochem. Biophys. Res. Commun. 293 (2002) 1377–1382.
[38] L. Zhong, M. Chiusa, A.G. Cadar, A. Lin, S. Samaras, J.M. Davidson, C.C. Lim, Targeted inhibition of ANKRD1 disrupts sarcomeric ERK-GATA4 signal transduction and abrogates phenylephrine-induced cardiomyocyte hypertrophy, Cardiovasc. Res. (2015) cvv108.
[39] N. Pescador, D. Villar, D. Cifuentes, M. Garcia-Rocha, A. Ortiz-Barahona, S. Vazquez, A. Ordoñez, Y. Cuevas, D. Saez-Morales, M.L. Garcia-Bermejo, Hypoxia promotes glycogen accumulation through hypoxia inducible factor (HIF)-mediated induction of glycogen synthase 1, PLoS One 5 (2010) e9644.
[40] S. Fisch, S. Gray, S. Heymans, S.M. Haldar, B. Wang, O. Pfister, L. Cui, A. Kumar, Z. Lin, S. Sen-Banerjee, Kruppel-like factor 15 is a regulator of cardiomyocyte hypertrophy, Proc. Natl. Acad. Sci. 104 (2007) 7074–7079.
[41] S.M. Haldar, Y. Lu, D. Jeyaraj, D. Kawanami, Y. Cui, S.J. Eapen, C. Hao, Y. Li, Y.-Q. Doughman, M. Watanabe, Klf15 deficiency is a molecular link between heart failure and aortic aneurysm formation, Sci. Transl. Med. 2 (2010) (26ra26-26ra26).
[42] T.-T. Hong, J.W. Smyth, D. Gao, K.Y. Chu, J.M. Vogan, T.S. Fong, B.C. Jensen, H.M. Colecraft, R.M. Shaw, BIN1 localizes the L-type calcium channel to cardiac T-tubules, PLoS Biol. 8 (2010) e1000312.
[43] T. Hong, H. Yang, S.-S. Zhang, H.C. Cho, M. Kalashnikova, B. Sun, H. Zhang, A. Bhargava, M. Grabe, J. Olgin, Cardiac BIN1 folds T-tubule membrane, controlling ion flux and limiting arrhythmia, Nat. Med. 20 (2014) 624–632.
[44] E. Lee, M. Marcucci, L. Daniell, M. Pypaert, O.A. Weisz, G.-C. Ochoa, K. Farsad, M.R. Wenk, P. De Camilli, Amphiphysin 2 (Bin1) and T-tubule biogenesis in muscle, Science 297 (2002) 1193–1196.
[45] C. Chiu, M. Tebo, J. Ingles, L. Yeates, J.W. Arthur, J.M. Lind, C. Semsarian, Genetic screening of calcium regulation genes in familial hypertrophic cardiomyopathy, J. Mol. Cell. Cardiol. 43 (2007) 337–343.
[46] Q. Xiao, A.E. Pepe, G. Wang, Z. Luo, L. Zhang, L. Zeng, Z. Zhang, Y. Hu, S. Ye, Q. Xu, Nrf3-Pla2g7 interaction plays an essential role in smooth muscle differentiation from stem cells, Arterioscler. Thromb. Vasc. Biol. 32 (2012) 730–744.
[47] B.S. Sutton, D.R. Crosslin, S.H. Shah, S.C. Nelson, A. Bassil, A.B. Hale, C. Haynes,

P.J. Goldschmidt-Clermont, J.M. Vance, D. Seo, Comprehensive genetic analysis of the platelet activating factor acetylhydrolase (PLA2G7) gene and cardiovascular disease in case–control and family datasets, Hum. Mol. Genet. 17 (2008) 1318–1328.
[48] U. Singh, S. Zhong, M. Xiong, T.-b. Li, A. Sniderman, T. Ba-Bie, Increased plasma non-esterified fatty acids and platelet-activating factor acetylhydrolase are associated with susceptibility to atherosclerosis in mice, Clin. Sci. 106 (2004) 421–432.
[49] I. Koskivirta, Z. Kassiri, O. Rahkonen, R. Kiviranta, G.Y. Oudit, T.D. McKee, V. Kytö, A. Saraste, E. Jokinen, P.P. Liu, Mice with tissue inhibitor of metalloproteinases 4 (Timp4) deletion succumb to induced myocardial infarction but not to cardiac pressure overload, J. Biol. Chem. 285 (2010) 24487–24493.
[50] M.-C. Kienitz, K. Bender, R. Dermietzel, L. Pott, G. Zoidl, Pannexin 1 constitutes the large conductance cation channel of cardiac myocytes, J. Biol. Chem. 286 (2011) 290–298.
[51] F.B. Chekeni, M.R. Elliott, J.K. Sandilos, S.F. Walk, J.M. Kinchen, E.R. Lazarowski, A.J. Armstrong, S. Penuela, D.W. Laird, G.S. Salvesen, Pannexin 1 channels mediate/find-me/'signal release and membrane permeability during apoptosis, Nature 467 (2010) 863–867.
[52] X. Yang, R. Khosravi-Far, H.Y. Chang, D. Baltimore, Daxx, a novel Fas-binding protein that activates JNK and apoptosis, Cell 89 (1997) 1067–1076.
[53] S.J. Charette, J.N. Lavoie, H. Lambert, J. Landry, Inhibition of Daxx-mediated apoptosis by heat shock protein 27, Mol. Cell. Biol. 20 (2000) 7602–7612.
[54] W.P. Tsang, T.W. Wong, H.H. Cheung, T.Y. Tsang, S.K. Kong, T.T. Kwok, Oncogene AF1q enhances doxorubicin-induced apoptosis through bad-mediated mitochondrial apoptotic pathway, Mol. Cancer Ther. 7 (2008) 3160–3168.
[55] D. Kumar, P. Gokhale, C. Broustas, D. Chakravarty, I. Ahmad, U. Kasid, Expression of SCC-S2, an antiapoptotic molecule, correlates with enhanced proliferation and tumorigenicity of MDA-MB 435 cells, Oncogene 23 (2004) 612–616.
[56] A. Singh, G. Ling, A.N. Suhasini, P. Zhang, M. Yamamoto, A. Navas-Acien, G. Cosgrove, R.M. Tuder, T.W. Kensler, W.H. Watson, Nrf2-dependent sulfiredoxin-1 expression protects against cigarette smoke-induced oxidative stress in lungs, Free Radic. Biol. Med. 46 (2009) 376–386.
[57] M. Kobayashi, M. Yamamoto, Molecular mechanisms activating the Nrf2-Keap1 pathway of antioxidant gene regulation, Antioxid. Redox Signal. 7 (2005) 385–394.
[58] D.M. Townsend, S-glutathionylation: indicator of cell stress and regulator of the unfolded protein response, Mol. Interv. 7 (2007) 313.
[59] T. Nakagawa, H. Zhu, N. Morishima, E. Li, J. Xu, B.A. Yankner, J. Yuan, Caspase-12 mediates endoplasmic-reticulum-specific apoptosis and cytotoxicity by amyloid-β, Nature 403 (2000) 98–103.
[60] C. Xu, B. Bailly-Maitre, J.C. Reed, Endoplasmic reticulum stress: cell life and death decisions, J. Clin. Investig. 115 (2005) 2656–2664.
[61] A.R. Marks, Calcium cycling proteins and heart failure: mechanisms and therapeutics, J. Clin. Investig. 123 (2013) 46–52.
[62] G. Sutendra, P. Dromparis, P. Wright, S. Bonnet, A. Haromy, Z. Hao, M.S. McMurtry, M. Michalak, J.E. Vance, W.C. Sessa, The role of Nogo and the mitochondria–endoplasmic reticulum unit in pulmonary hypertension, Sci. Transl. Med. 3 (2011) (88ra55-88ra55).
[63] J. Hu, Y. Shibata, C. Voss, T. Shemesh, Z. Li, M. Coughlin, M.M. Kozlov, T.A. Rapoport, W.A. Prinz, Membrane proteins of the endoplasmic reticulum induce high-curvature tubules, Science 319 (2008) 1247–1250.
[64] I. Dalle-Donne, D. Giustarini, R. Rossi, R. Colombo, A. Milzani, Reversible S-glutathionylation of Cys 374 regulates actin filament formation by inducing structural changes in the actin molecule, Free Radic. Biol. Med. 34 (2003) 23–32.
[65] F.C. Chen, O. Ogut, Decline of contractility during ischemia-reperfusion injury: actin glutathionylation and its effect on allosteric interaction with tropomyosin, Am. J. Physiol.-Cell Physiol. 290 (2006) C719–C727.
[66] B. Wang, S.M. Haldar, Y. Lu, O.A. Ibrahim, S. Fisch, S. Gray, A. Leask, M.K. Jain, The Kruppel-like factor KLF15 inhibits connective tissue growth factor (CTGF) expression in cardiac fibroblasts, J. Mol. Cell. Cardiol. 45 (2008) 193–197.
[67] S. Hein, E. Arnon, S. Kostin, M. Schönburg, A. Elsässer, V. Polyakova, E.P. Bauer, W.-P. Klövekorn, J. Schaper, Progression from compensated hypertrophy to failure in the pressure-overloaded human heart structural deterioration and compensatory mechanisms, Circulation 107 (2003) 984–991.
[68] D. Han, A.G. Lerner, L.V. Walle, J.-P. Upton, W. Xu, A. Hagen, B.J. Backes, S.A. Oakes, F.R. Papa, IRE1α kinase activation modes control alternate endoribonuclease outputs to determine divergent cell fates, Cell 138 (2009) 562–575.
[69] A.G. Lerner, J.-P. Upton, P. Praveen, R. Ghosh, Y. Nakagawa, A. Igbaria, S. Shen, V. Nguyen, B.J. Backes, M. Heiman, IRE1α induces thioredoxin-interacting protein to activate the NLRP3 inflammasome and promote programmed cell death under irremediable ER stress, Cell Metab. 16 (2012) 250–264.